Int. J. Electrochem. Sci., 12 **(2017)** 8381 – 8398, doi: 10.20964/2017.09.40

International Journal of
ELECTROCHEMICAL
SCIENCE
www.electrochemsci.org

High Performance of Pb-doped $Li_4Ti_5O_{12}$ as an Anode Material for Lithium Ion Batteries

Keqiang Ding[1,*], *Binjuan Wei*[1], *Yan Zhang*[1], *Chenxue Li*[1], *Xiaomi Shi*[1], *Junqing Pan*[2,*]

[1] College of Chemistry and Materials Science, Hebei Normal University, Shijiazhuang, Hebei 050024, P.R. China
[2] State Key Laboratory of Chemical Resource Engineering, Beijing University of Chemical Technology, Beijing, 100029, P.R. China
[*]E-mail: dkeqiang@263.net, jqpan@mail.buct.edu.cn

Received: 13 May 2017 / *Accepted:* 6 July 2017 / *Published:* 13 August 2017

For the first time, Pb-doped $Li_4Ti_5O_{12}$ (Pb-LTO) was prepared by a solution-drying-calcination (SDC) method in which lead acetate was employed as a dopant. In the present work, the effect of Pb to Ti atomic ratio on the physicochemical properties as well as the electrochemical performance of the synthesized materials was systematically investigated. X-ray diffraction (XRD), scanning electron microscopy (SEM), cyclic voltammometry (CV), electrochemical impedance spectroscopy (EIS) and galvanostatic charge-discharge test were mainly used to examine the as-prepared samples. XRD results not only effectively demonstrated the formation of $Li_4Ti_5O_{12}$ but also indicated that the crystallinities of the resultant samples were closely related to the Pb to Ti atomic ratio used. Also, SEM images indicated that relatively regular particles with an average size of 0.5 μm could be prepared when the Pb to Ti atomic ratio was 0.01 (sample b). The results of electrochemical measurements indicated that the initial discharge capacity of sample b was as high as 185 mAh g^{-1} at 0.2C rate and sample b could show a high specific capacity of 169 mAh g^{-1} after 20 cycles at 0.2 C rate. Using a very cheaper dopant of lead acetate to prepare the high performance Pb-doped LTO was the main contribution of this preliminary work, which was believed to be very beneficial to the further commercialization of LTO.

Keywords: $Li_4Ti_5O_{12}$; lead acetate; Pb doping; anode materials; lithium ion batteries

1. INTRODUCTION

Although lithium-ion batteries (LIBs) as one kind of the most important power sources have been successfully commercialized in some electric vehicles and portable electronics mainly due to their higher operating voltage and higher energy density, some issues like the safety issue and higher prices still greatly impeded their further applications [1]. The safety issue of LIBs, which is mainly

caused by the formation of metallic lithium on the anode surface, was regarded as the most key problem among all the issues of LIBs, since it might lead to some unpredictable injuries under some special conditions [2]. Thus, developing novel anode materials, which can replace the current commercial anode material of graphite while maintaining an acceptable electrochemical performance, has turned into a key topic for the LIBs-related researchers.

So far, many novel anode materials have been developed with an intention to solve above mentioned problems. These newly developed anode materials, besides Fe_2O_4-based materials [3], mainly included two groups, i.e., some metal oxides like SnO_2 [4] and Fe_2O_3 [5], and some elementary substances such as silicon [6] and tin [7]. Although a large number of novel anode materials have been successfully prepared, the reports concerning the practical applications of these newly produced anode materials are very rare, which was mainly caused by their poor electrochemical performances, complicated preparation processes or the higher preparation costs. Among these newly developed anode materials, lithium titanate ($Li_4Ti_5O_{12}$, LTO) was thought as one of the most promising anode materials for LIBs because of its following superior characterizations [8,9]: (1) The Li-insertion voltage (ca. 1.5 V vs. Li^+/Li) of LTO is much higher than that of graphite (0.2 V vs. Li^+/Li), which can efficiently avoid the formation of elementary lithium and the reduction reaction of the electrolyte on the surface of the electrode and the formation of a SEI (solid electrolyte interphase) layer; (2) LTO is generally called as a zero-strain insertion material, which shows almost no structural variation during the lithium ions insertion/extraction processes, being very beneficial to the improvement of the reversibility and cycling capability of a LTO-based LIBs. However, as claimed recently, the electronic conductivity and ionic conductivity of LTO were very poor which remarkably hampered the further commercialization of LTO. Therefore, numerous strategies have been developed for enhancing the electrochemical behavior of LTO. To our knowledge, doping carbon or metals into LTO was reckoned as the most feasible approach for promoting the electrochemical properties of LTO, mainly due to the simple procedure and lower preparation cost as compared to other proposed approaches. Many kinds of metals such as Ce [10], Ag [11], Ce [12], Gd [13], etc., have been employed to produce metal-doped LTO, exhibiting enhanced electrochemical performance. Evidently, the doping of noble metals into LTO will definitely increase the preparation cost of LTO which is not favorable to the final commercialization of LTO. In fact, simple preparation process and lower producing cost as well as the acceptable property are the main three factors for the large scale production of a novel material. Lead (Pb), as an abundant and cheaper metal, has been successfully commercialized in the traditional lead acid battery. However, to the best of our knowledge, no paper reporting the preparation of Pb-doped LTO using a solution-drying-calcination (SDC) method is published so far.

In the present work, for the first time, Pb-doped $Li_4Ti_5O_{12}$ (LTO) was prepared using lead acetate as the dopant by a SDC method. The influence of Pb to Ti atomic ratio on the properties of synthesized samples was systematically investigated. The results of electrochemical measurements indicated that when the Pb to Ti atomic ratio was 0.01, the best electrochemical behavior was exhibited by the prepared material, showing a high specific capacity of 169 mAh g^{-1} after 20 cycles at 0.2 C rate.

2. EXPERIMENTAL

2.1. Materials

Lead acetate ($Pb(Ac)_2$), lithium acetate ($LiAc{\cdot}2H_2O$), tetrabutyl titanate $[CH_3(CH_2)_3O]_4Ti$ and other used reagents were all purchased from Tianjin Chemical Reagent Co. Ltd. All materials used in the battery testing, like acetylene black, polytetrafluoroethylene (PTFE) binder, electrolyte of 1 M $LiPF_6$ and the cell, were all bought from the Tianjin Lianghuo S&T Developing Co. Ltd. All the chemicals were of analytical grade and used as-bought without any further purification.

2.2. Preparation of Pb-doped LTO

Firstly, the starting materials of $LiAc{\cdot}2H_2O$, $Pb(Ac)_2$ and $[CH_3(CH_2)_3O]_4Ti$ were weighed carefully at the atomic ratio of Li: Ti: Pb = 0.85:1: 0.005 to prepare sample a. A proper amount of well weighed $LiAc{\cdot}2H_2O$ and $Pb(Ac)_2$ were dissolved in an amount of deionized water to produce a solution (solution 1). And meanwhile, an amount of $[CH_3(CH_2)_3O]_4Ti$ was transferred into 40 mL of anhydrous ethanol generating a solution (solution 2). And then, solution 2 was put into solution 1 dropwise under a vigorous stirring, generating a white colloid solution. Subsequently, the produced white colloid was put in an air dry oven and dried at 150 °C for about 4 h, leading to the formation a precursor. And then, the resultant precursors were thoroughly milled in an agate mortar forming some tiny powders, and afterwards, the produced powders were pressed into tablets by a manual tablet machine, lastly, the synthesized tablets were transferred into an electronic furnace and sintered at 800 °C for 10 h under the air condition. When producing other samples, the amounts of $LiAc{\cdot}2H_2O$ and $[CH_3(CH_2)_3O]_4Ti$ were maintained constant (the atomic ratio of Li to Ti was kept at 0.85:1) and the amount of $Pb(Ac)_2$ varied correspondingly to study the influence of atomic ratio of Pd to Ti on the properties of the resultant samples. The prepared samples with the atomic ratios of Pb to Ti 0.005, 0.01, 0.015 and 0.02 were, respectively, denoted as sample a, b, c and d.

2.3. Characterization

The crystal structure, particle morphology and element components of the as-prepared samples were examined by using X-ray diffraction (Bruker AXS, D8 ADVANCE, Germany), scanning electron microscopy (HITACHI, SEM S-570) and Energy dispersive spectrometer (EDS, INCA Energy 350, England), respectively. Fourier transform infrared spectrometry (FTIR) measurements were carried out on a Hitachi FT-IR 8900 spectrometer (Japan). X-ray photoelectron spectroscopy (XPS, Kratos Analytical spectrometer, Al $K_{\square}$ radiation) was utilized to feature the chemical composition of the prepared samples. The Renishaw InVia Micro-Raman Spectroscopy System with an excitation wavelength of 514 nm was used to finish the measurement of Room temperature Raman spectra.

Electrochemical measurements, mainly including Cyclic Voltammetry (CV), Electrochemical Impedance Spectroscopy (EIS), were performed on a personal computer-controlled CHI 660B electrochemical workstation (Shanghai Chenhua Apparatus, China). In the EIS measurement, the

oscillation voltage applied to the cells and the employed frequency range were 5 mV and 100 kHz-0.1 Hz, respectively. All the experiments were conducted at room temperature.

The working electrodes were carefully prepared according to the following steps. (1) The formation of slurry. The active materials, acetylene black and polyvinylidene fluoride (PVDF) at the mass ratio of 8:1:1 were thoroughly mixed in an agate mortar to form a mixture, and then, several drops of N-methyl-2-pyrro-lidone (NMP) were dropped into the prepared mixture, generating slurries. And then the obtained slurry was uniformly covered on a well-treated aluminum foil using a glass piece and dried in a vacuum drying oven at 120°C for 6 h, producing a working electrode. The working electrodes assembled by sample a, b, c and d were denoted as electrode a, b, c and d, respectively. The half-cell was contained in a 2032 coin-type cell (20 mm in diameter and 32 mm in thickness), which was assembled in a high purity nitrogen filled glove box. The half-cells, namely, two-electrode electrochemical cells, besides the prepared working electrode, mainly consisted of lithium metal foil as the negative electrode, Celgard 2400 separator and an electrolyte of 1 M $LiPF_6$ in ethylene carbonate (EC):dimethyl carbonate (DEC): ethyl methyl carbonate (EMC) (1:1:1, vol.). Evidently, here, metallic lithium foils were used as both the reference and counter electrodes. The galvanostatic charge-discharge tests were performed using a battery testing system (CT-3008W-5V20mA-S4, Shenzhen Neware Electronics Co., Ltd. China) at various current rates between 0.5 and 2.5 V at room temperature. The theoretical capacity value of LTO is calculated to be 175 mAh g^{-1}.

3. RESULTS AND DISCUSSION

3.1 XRD analysis

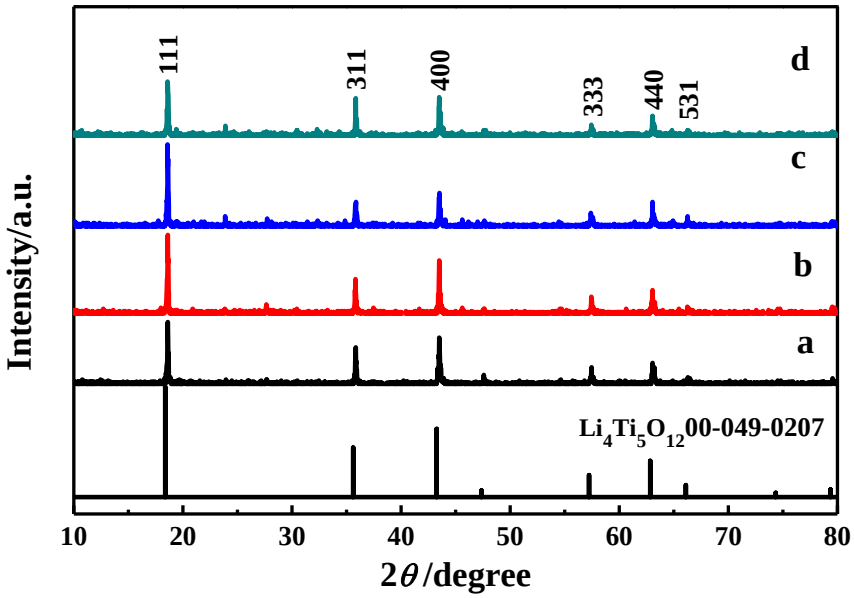

Figure 1. XRD patterns of all the synthesized samples. Pattern a, b, c and d correspond to sample a, b, c, and d. The standard XRD pattern for LTO was also presented.

Fig. 1 shows the XRD patterns of all prepared samples including the standard pattern of LTO. Evidently, the main diffraction peaks corresponding to $Li_4Ti_5O_{12}$ (JCPDS no. 00-049-0207), i.e., six typical diffraction peaks of at 18.5° (111), 35.8° (311), 43.5° (400), 57.1° (511), 62.8° (440) and 66.0° (531), are clearly exhibited [14]. It strongly indicated that the main components of all prepared samples were LTO, which could be indexed to a cubic spinel structure with the space group of *F*d-3m [14]. This result also proved that the doped lead did not deteriorate the main crystal structure of the prepared LTO. Also, some weak diffraction peaks assigned to TiO_2 were displayed, suggesting the existence of TiO_2 in the final samples. Interestingly, no diffraction peaks of lead oxides were observed, which probably was due to their lower amounts. Apparently, the intensity of the diffraction peaks changed remarkably with the Pb to Ti atomic ratio. It is clear that sample b delivered the highest diffraction peaks among all the prepared materials. Generally, the higher diffraction peaks corresponded to a better crystallinity [15]. Thus, it can be inferred that sample b had the best crystallinity among all the synthesized samples. In addition, the intensity ratios of $I_{(311)}/I_{(111)}$ for sample a, b, c and d were estimated to be 0.642, 0.421, 0.250 and 0.692, respectively. Evidently, the intensity ratio of $I_{(311)}/I_{(111)}$ for sample b was very close to that of the standard XRD pattern of LTO (0.423), which implied that the crystal structure of sample b was very close to that of the standard LTO, having a well-defined crystal structure. Generally, the well-defined crystal structure of an anode material was favorable to the directional transfer of both electron and lithium ions, basing on our previous work [16].

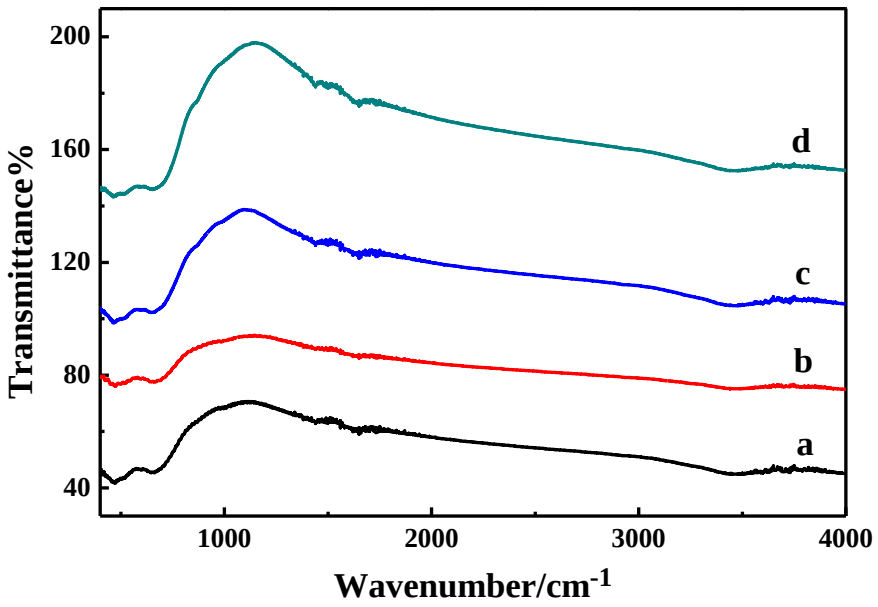

Figure 2. FTIR spectra for the as-synthesized samples. Spectrum a, b, c and d correspond to sample a, b, c and d.

To further assure the formation of Pb-doped LTO, the FTIR spectra of all synthesized materials were measured and the results are shown in Fig.2. Apparently, all the FTIR curves showed similar

shape which effectively verified that similar functional groups were contained in all prepared samples. As addressed previously, the absorption band centered at 660 cm^{-1} should be resulted from the MO_6 (TiO_6) octahedron [17]. The absorption peaks of at 660 cm^{-1} were clearly displayed by all samples which substantially demonstrated that the main components of all resultant samples were LTO. The weak and small absorption bands positioned at 1430~1635 cm^{-1} and 3400 cm^{-1} should be assigned to the C-O and -OH groups, respectively, according to the former work [18]. It was reported that the C-O and -OH groups were mainly originated from the adsorbed CO_2 and H_2O on the surface of LTO in the air [19]. Close observation indicated that sample b showed the smallest absorption peak of at 1430~1635 cm^{-1} and 3400 cm^{-1} among all the prepared samples, which demonstrated that the impurity content of sample b was lower as compared to other samples. This result was consistent with the analysis from the XRD pattern (Fig.1) that sample b had a well-defined crystal structure.

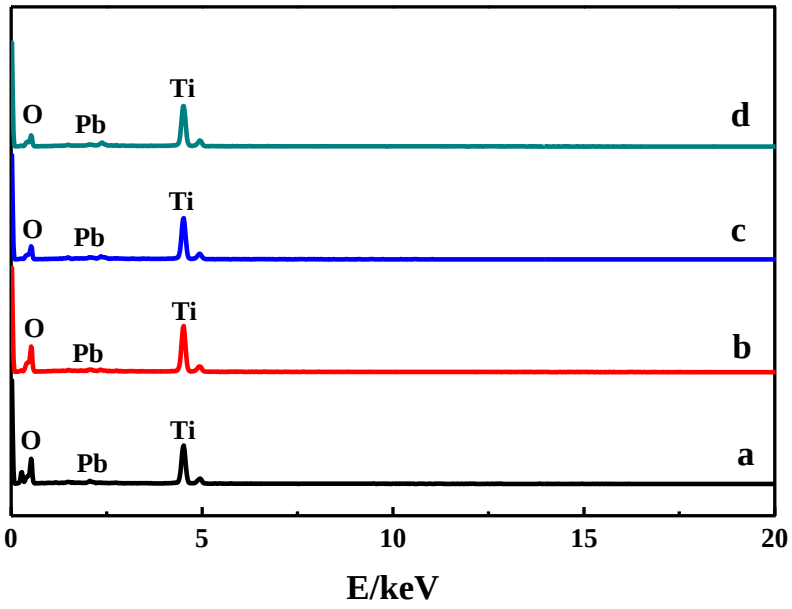

Figure 3. EDS spectra for all the resultant samples. Pattern a, b, c and d correspond to sample a, b, c and d.

To confirm the element compositions of the prepared materials, EDS analysis was conducted and the results are presented in Fig.3. For all the samples, the peaks corresponding to the elements of O, Pb and Ti were clearly displayed. The atomic ratios of Pb to Ti for sample a, b, c and d were measured to be 0.003, 0.010, 0.018 and 0.021, respectively. It implied that the atomic ratio of Pb to Ti in the final products was not coincident with that in the starting materials, which was probably due to the loss of substances in the preparation process. The EDS results strongly demonstrated that Pb has been successfully transferred into the final products using lead acetate as the precursor via a SDC method.

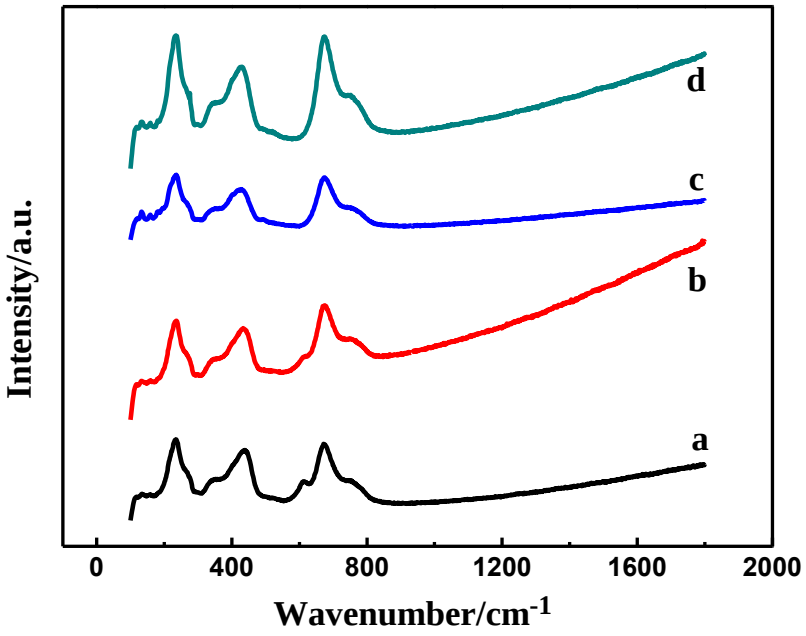

Figure 4. Raman spectra of the synthesized samples. Curve a, b, c and d correspond to sample a, b, c and d.

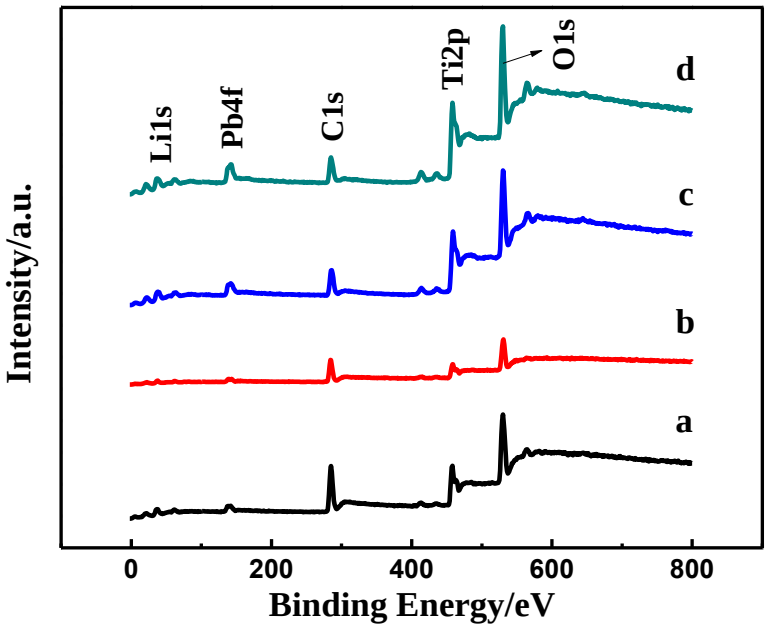

Figure 5a. Wide scan XPS spectra for all the samples prepared. Curve a, b, c and d corresponded to sample a, b, c and d.

Raman spectroscopy of all synthesized samples was also measured with an intention to detect the main groups in the final samples, and the results are illustrated in Fig. 4. Apparently, three typical peaks located at about 231, 431, 670 cm^{-1} were respectively displayed clearly. According to the former report [20], the higher frequency band of at 670 cm^{-1} was originated from the vibration of Ti-O bonds in TiO_6 octahedra. And the bands appearing at about 431 cm^{-1} were from the stretching vibrations of

the Li-O bonds in LiO_4 and LiO_6 polyhedra. This result substantially proved that all the vibration characteristics of LTO were not destroyed by the doped Pb, and the main LTO structure was maintained in the prepared materials, according well with the XRD results (Fig.1).

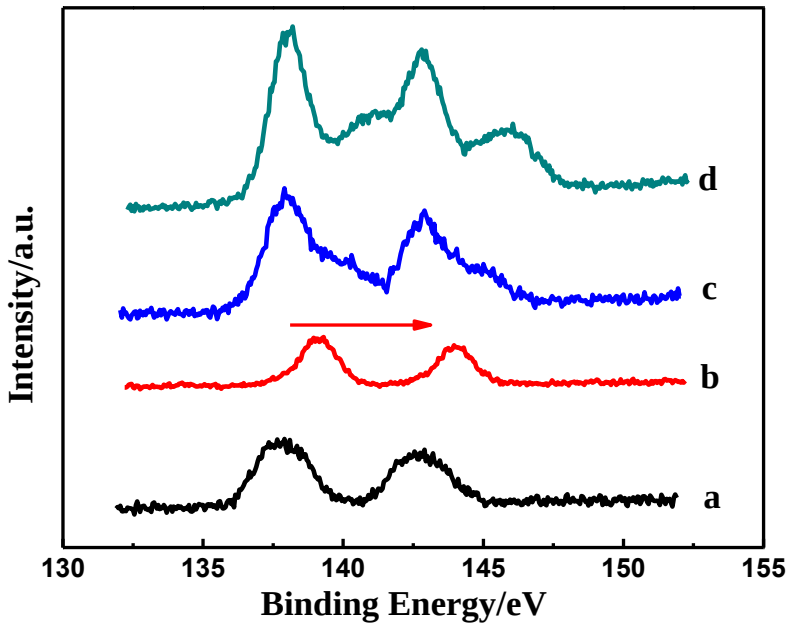

Figure 5b. High resolution XPS spectra of Pb element for the prepared samples. Curve a, b, c and d corresponded to sample a, b, c and d.

XPS survey spectra for all samples are given in Fig. 5a and 5b, desiring to further confirm the valences of elements in the resultant samples. Apparently, the wide scan XPS spectra of Fig.5a have strongly confirmed the presence of Li, Pb, C, Ti and O elements in all prepared samples. The presence of spin-orbit doublets of Ti2p firmly evidenced the presence of Ti^{4+} oxidation state in the final samples [21]. Also, the O1s peak positioned at 530.2 eV assured the formation of the Ti-O bonding in a spinel LTO structure [22]. As shown in Fig.5b, the peaks located at about 137.5 eV and 142.1 eV were the characters of Pb $4f_{7/2}$ and Pb $4f_{5/2}$ in Pb 4f spectra for PbO, basing on the previous work concerning Pb [23]. Close observation revealed that the peak positions for both Pb $4f_{7/2}$ and Pb$4f_{5/2}$ were almost identical for sample a, c and d, and the binding energies (BE) of above two peaks for sample b were shifted positively for about 1.1eV as compared to sample a, c and d. It was claimed that the BE shift in oxide compound was mainly due to the rearrangement of electronic charge around the constituent atoms [24]. That is to say, the newly formed electric charge distribution of sample b was different from other three samples, which might affect the lithium ions migration leading to an enhanced electrochemical performance. Evidently, the presence of carbon in the synthesized samples was from the organic group of the starting materials. Thus, strictly speaking, the prepared samples were Pb and C co-doped LTO materials.

3.2 Morphology characterization

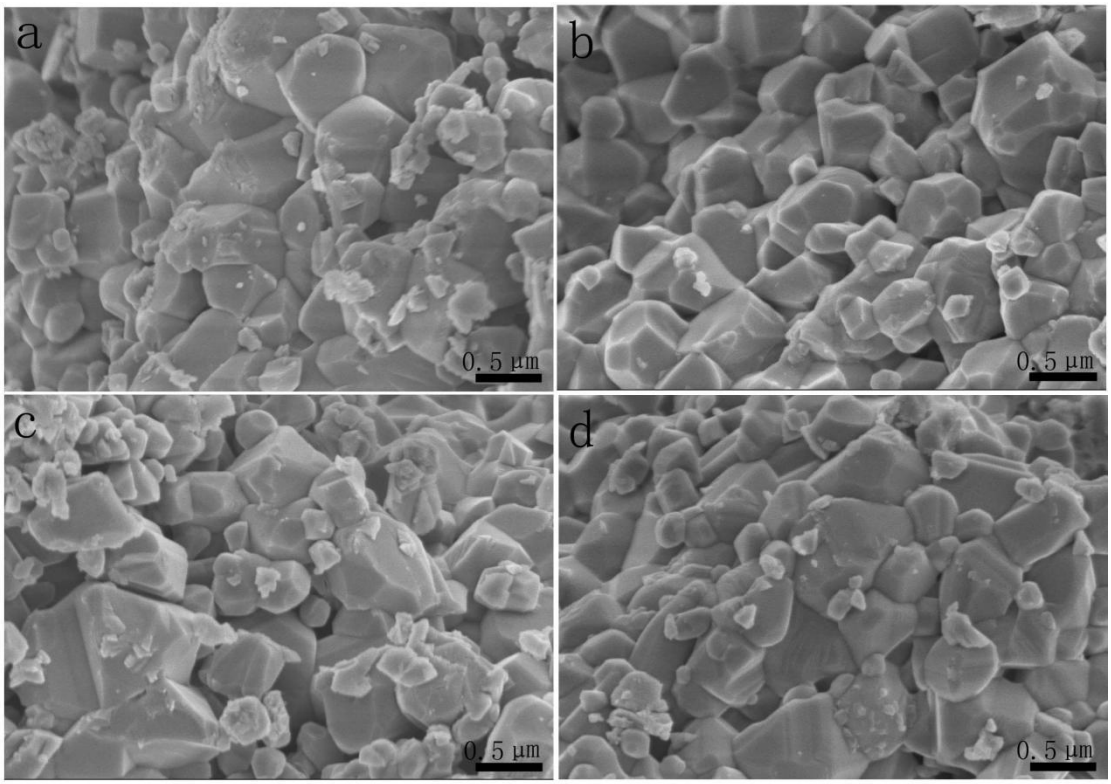

Figure 6. SEM images of the resultant samples. Image a, b, c and d correspond to sample a, b, c and d. The direct magnification was 30.0K.

Fig.6 shows the SEM images of all prepared materials. It is evident that more larger and regular particles were exhibited by sample b. While for sample a, c and d, some irregular and smaller particles are found to be immobilized on the regular and larger particles. Probably, these irregular and smaller particles were the impurities prepared. Also, it is clear that the particle size distribution of sample b was more uniform as compared to sample a, c and d. The particle size ranges for sample **a**, **b**, **c** and **d** were roughly evaluated to be 150~850 nm, 200~700 nm, 200~900 nm and 150~800 nm, respectively. And the average particle sizes for sample **a**, **b**, **c** and **d** were 650 nm, 500 nm, 700 nm and 650 nm, respectively. Thus, the particle size of sample b was smaller than other samples. Generally, the smaller particle was favorable to the diffusion of lithium ions due to the shortened diffusion path way. This result effectively indicated that the doping of Pb into the starting materials has greatly affected the morphologies, the particle size and the particle size distribution of the prepared samples. According to our previous work [16], the regular crystal structure of an anode electrode material was beneficial to the directional transfer of lithium ions, and the presence of impurities in the prepared materials was detrimental to lithium ion shifting, thus, sample b, due to its well defined crystal structure, may present a satisfied electrochemical performance when compared to other samples.

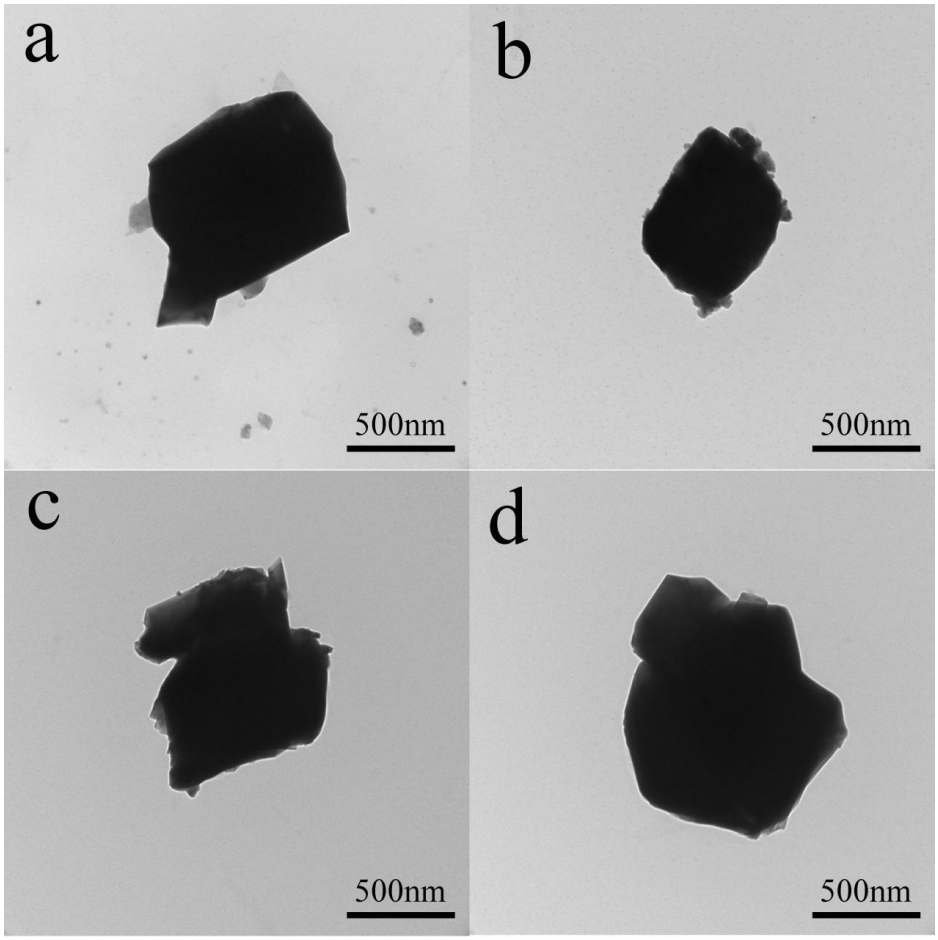

Figure 7. TEM images for the prepared samples. Image a, b, c and d corresponded to sample a, b, c and d. The direct magnification was 80K.

TEM microstructures of all synthesized samples are provided in Fig.7. Interestingly, for all the samples, regular particles are observed clearly. It strongly demonstrated that all the large particles appearing in Fig.6 were constructed by smaller and regular crystal particles. Also, this result implied that all prepared samples had better crystallinity, which was consistent with the results shown by XRD patterns (Fig.1). The particle sizes for sample a, b, c and d were approximately estimated to be 650 nm, 500 nm, 650 nm and 750 nm, respectively. That is to say, sample b had the smallest particle size among all the prepared samples. It should be noted that the particle sizes of all prepared samples were much smaller than those of Zn-doped LTO [25] and ref.12. Generally, the property of smaller particle size may lead to the following superior properties: (1) The diffusion paths of lithium ions in the bulk electrode material would be greatly shortened by the lowered the particle size: (2) The lowered particle size would definitely increase the particle number when the loadings were identical, which would lead to an enhanced contacting area of the electrode/electrolyte interface. Consequently, the over-potentials of electrochemical reaction could be significantly lowered, which were very advantageous to the lithiation/delithiation processes, basing on the Tafel equation [26].

3.3 Electrochemical performance

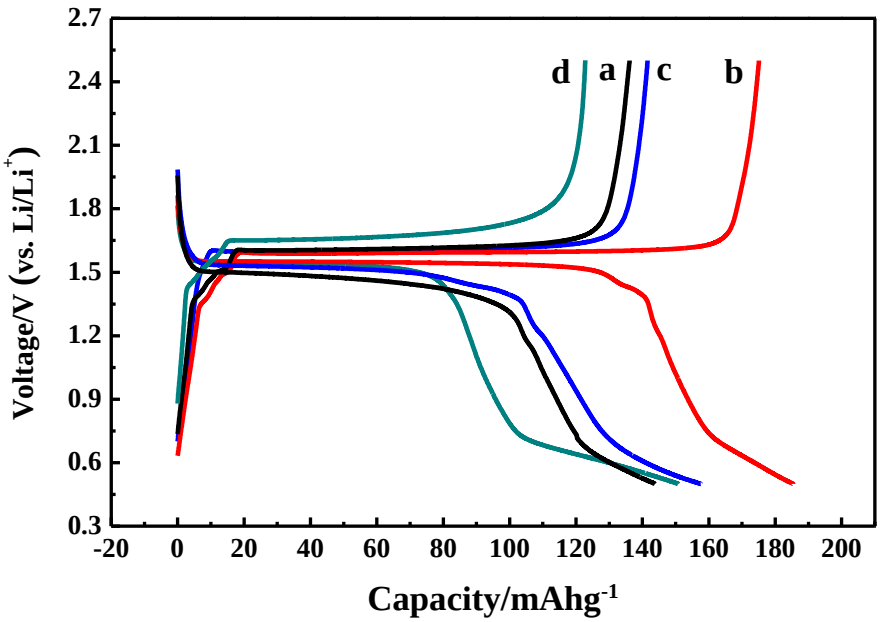

Figure 8a. The first galvanostatic charge-discharge curves of the as-synthesized samples obtained at 0.2C rate. The curves of a, b, c and d correspond to sample a, b, c and d.

Fig. 8a shows the initial charge and discharge curves of all prepared samples at 0.2C rate. The shapes of these curves are very close to that of pure LTO [27], which strongly indicated that the insertion and extraction mechanisms of the lithium ions in all materials were similar to that of LTO. On the basis of the previous work about LTO, the potential plateaus positioned at around 1.55 V and 1.60V should be discharging and charging potential plateau, respectively. Commonly, the presence of the potential plateaus in the charge and discharge profiles indicated a two-phase reaction between spinel structure of $Li_4Ti_5O_{12}$ and rock-salt structure of $Li_7Ti_5O_{12}$, basing on the former report [28]. The initial discharge capacities for sample a, b, c and d were estimated to be approximately 144, 185, 157 and 151 mAh g^{-1}, respectively. It indicted that a proper amount of Pb doped into LTO was beneficial for promoting the discharge capacity value of LTO. Sample b showed the largest specific capacity value among all the electrodes, which probably should be ascribed to its better crystallinity (Fig.1), smaller particle size (Fig.6 and Fig.7) and more uniform particle size distribution (Fig.6) as compared to other samples. Moreover, the discharge capacity of 185 mAh g^{-1} was significantly larger than the theoretical discharge capacity of pure LTO (1C =175 mAh g^{-1})[29], which was probably due to the fact that some impurities like TiO_2 and PbO also had the ability to accommodate Li ions. It should be noted that discharge capacity of 185 mAh g^{-1} of sample b was evidently larger than that of the LTO prepared by a spontaneous solid-liquid mixing process (160.1 mAh g^{-1} at 0.2C) [30]. That is to say, the discharge capacity value of sample b was superior or comparable to the previously reported data. Also, it must be emphasized that lead acetate was a very cheap raw material which could greatly cut down the preparation cost of metal doped LTO as compared to other noble metals like Gd [13].

Meanwhile, close observation of Fig. 8a revealed that the potential separations between the charge potential plateau and discharge potential plateau were very different from each other. The potential separation value, which was roughly estimated from the midpoint value of the discharge potential plateau, for half-cell a, b, c and d, were approximately 140, 50, 90 and 150 mV, respectively. Commonly, a smaller potential gap value corresponded to a lower over-potential value, thus, sample b had the smallest over-potential value which was very favorable to the improvement of the reversibility of a charge-discharge process. Also, it can be seen clearly that there is an inflection point in all discharge curves. As stated previously, the appearance of the inflection point was resulted from the decomposition of the electrolyte used in a battery [31]. The inflection point potentials for half-cell a, b, c and d were estimated to be 0.704, 0.724, 0.706 and 0.718 V, respectively. The highest value of inflection point for sample b indicated that the decomposition of the electrolyte did not easily take place in the case of sample b, though the differences in the inflection point potential were very slight. Thus, it can be concluded that the doped Pb could not only affect the reversibility of the charging-discharging process but also influence the decomposition performance of the electrolyte employed.

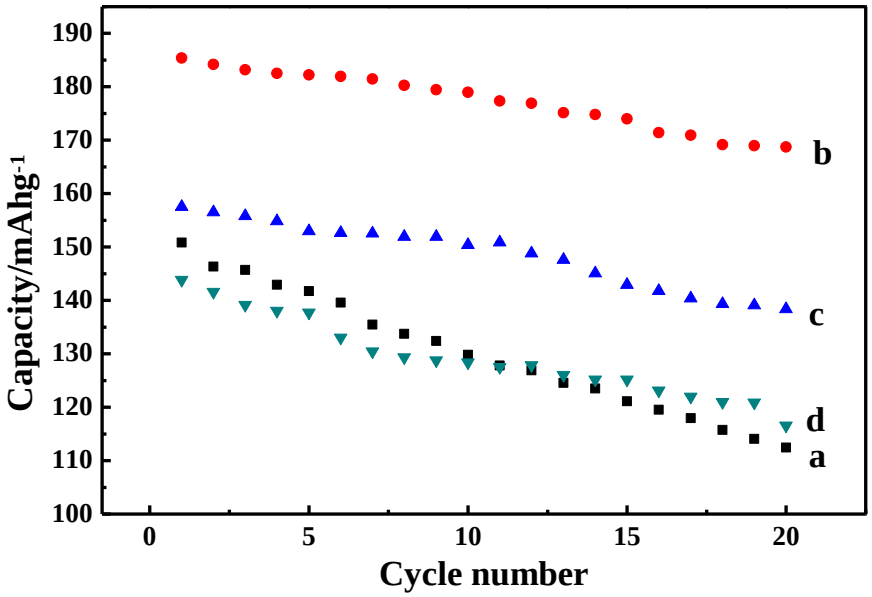

Figure 8b. Cycling performance of the as-prepared samples at the current density of 0.2C rate for 20 cycles.

It is well known that the cycling performance of an electrode material is an important factor which can be employed to directly determine the service life of a battery. The cycling performance profiles, i.e., the relationship between the discharge capacity and cycling number, were measured and the results are shown in Fig. 8b. Although the discharge capacity value decreased clearly with increasing the cycling number for all the electrodes, electrode b showed the largest discharge capacity value among all prepared samples in the whole testing period. The discharge capacities of the first cycle at 0.2 C rate were 151, 185, 157 and 144 mAh g^{-1} for sample a, b, c and d, respectively. And at the 20^{th} cycle, the discharge capacities for sample a, b, c and d were retained as high as 112, 168, 139

and 116 mAh g^{-1}, which were equal to 74.1 %, 89.2 %, 88.5 % and 80.6 % of the initial discharge capacity value, respectively. Therefore, sample b delivered the highest discharge capacity value as well as the largest capacity retention value among all prepared samples, showing the best cycling stability among all the prepared samples.

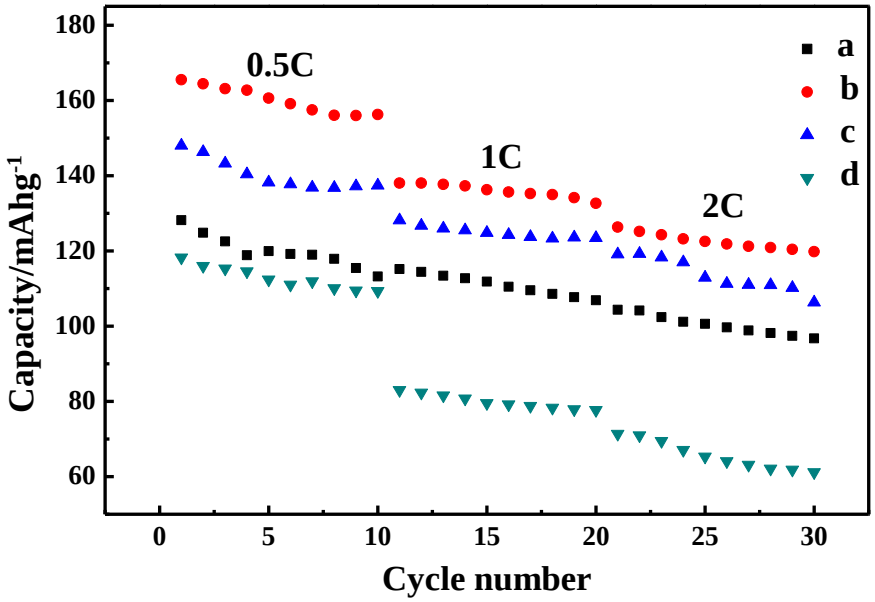

Figure 8c. The rate performance of all prepared samples. Each sample was respectively cycled 10 times at 0.2 C, 1C and 2C rate.

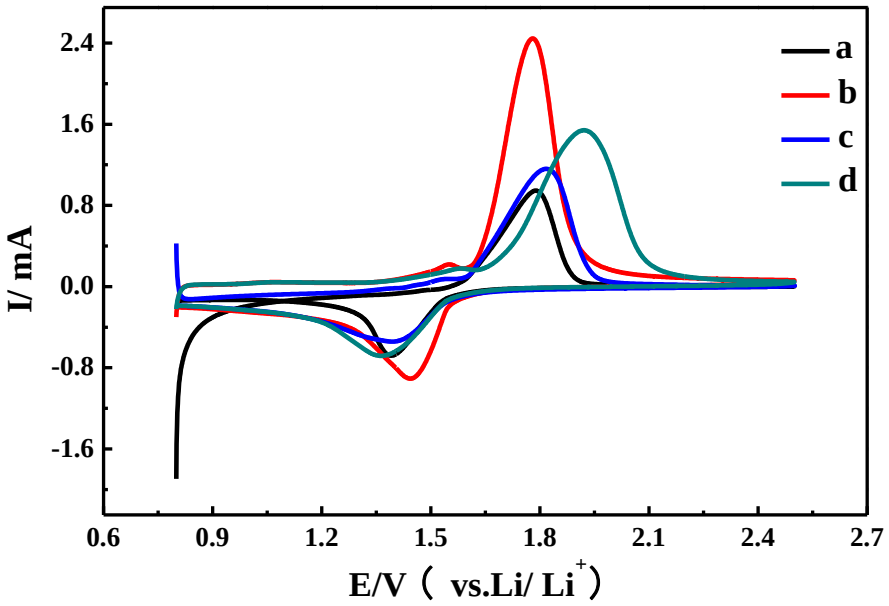

Figure 9a. Cyclic voltammograms of the prepared electrodes for the 1st cycle at a scan rate of 0.5mV s^{-1} between 0.8 and 2.50 V (vs. Li/Li^+) at room temperature.

To further examine the rate capability of the synthesized electrodes, the current rate applied was increased from 0.5 C to 2 C, and at each current rate the electrode was tested for 10 cycles and the results are illustrated in Fig.8c. It was clear that in the total rate testing periods, electrode b delivered the largest discharge capacity value among all prepared electrodes. For example, the discharge capacity at 2 C for electrode b was 120 mAh g^{-1} after 10 cycles, which was observably larger than that of other electrodes (the discharge capacity value for electrode a, c and d were 95, 104 and 61 mAh g^{-1}, respectively). That is to say, sample b had the best rate capability among all the resultant samples.

To further reveal the intercalation and de-intercalation behavior of lithium ions in the prepared samples, cyclic voltammetry (CV) curves were recorded in the potential range of 0.8V~ 2.5V at a scanning rate of 0.5 mV s^{-1} and the results are presented in Fig.9a. Interestingly, a pair of well-defined redox peak is displayed in all CV curves, which effectively implied that the intercalation and de-intercalation processes of lithium ions in all prepared materials could proceed very well. It was evident that the largest peak current was exhibited by sample b, which suggested that sample b had faster kinetics as compared to other samples [30]. Also, the peak area of a CV curve was approximately directly proportional to the charge consumed in the electrochemical reaction [31]. Here, apparently, the largest peak area of the CV curve was displayed by sample b, which indicated that the largest amount of charge was transferred in sample b, which might lead to the largest discharge capacity value as shown in Fig.8a, b and c. Meanwhile, the electrochemical parameter of the peak potential separation of ΔE_p ($\Delta E_p=E_{pa}-E_{pc}$) is also a key parameter which is closely related to the reversibility of an electrode reaction [32]. Basing on our previous work [32], generally, a smaller value of ΔE_p for a CV curve corresponded to a better reversibility of an electrochemical reaction. The ΔE_p values for sample a, b, c and d were roughly calculated to be 0.39V, 0.32V, 0.40V and 0.56V, respectively, That is to say, sample b may deliver a better reversibility and a less polarization potential when compared to other samples, which probably was attributed to its better crystallinity (Fig.1), smallest particle size (Fig.6), more uniform particle size distribution (Fig.6) and BE positive shifting (Fig.5b).

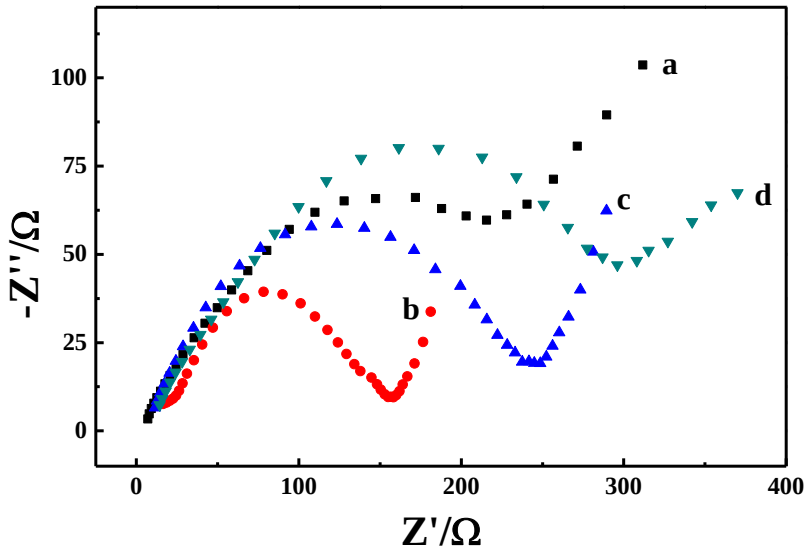

Figure 9b. Nyquist plots of electrochemical impedance of the half cells assembled by the prepared samples. Plots a, b, c and d correspond to the resultant sample a, b, c and d.

EIS, as a simple and intuitive method, has been widely employed in examining the electrochemical performance of a lithium ions battery, as reported previously [33]. Nyquist plots, one typical curve of EIS, recorded after 20 cycle test, are illustrated in Fig. 9b. It should be stressed that all the curves were recorded respectively at their open circuit potentials. Commonly, for a typical Li half-cell, the intercept at the Z_{real} (here is Z') axis in the highest frequency region was from the total resistance which was called as the ohmic resistance (R_{Ω}) [34]. And the depressed semicircle appearing in the high-to-middle frequency range, generally, corresponded to a parallel circuit that contained a resistance element and a capacitor element, and for a typical Li half-cell, the length of the diameter of the semicircle was directly proportional to the value of charge transfer resistance (R_{ct}). The sloped line appearing in the lower frequency region was originated from the limited diffusion of lithium ions into the electrode materials. Among above three parameters, the parameter of R_{ct} is the most valuable factor which can be used to compare the kinetics of different half-cells directly. The values of R_{ct} for electrode a, b, c and d were roughly evaluated to 312 Ω, 160 Ω, 261 Ω and 341 Ω, respectively. Commonly, smaller value of $R_{ct,}$ corresponded to a faster kinetics process of an electrode reaction. Hence, electrode b had the fastest lithium insertion/extraction kinetics among all the electrodes, which might account for the better electrochemical performance of sample b as compared to other samples.

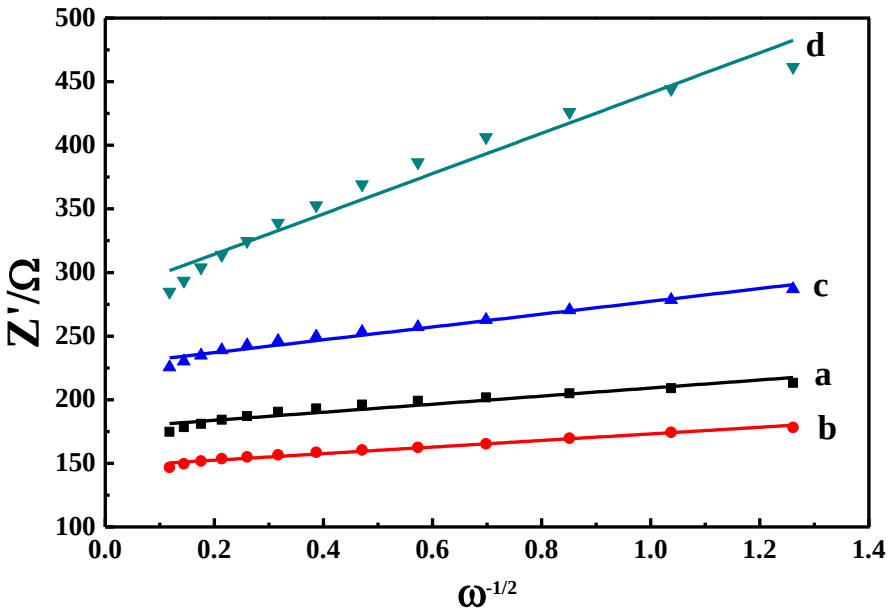

Figure 9c. Graph of Z' plotted against $\omega^{-1/2}$ at the low frequency region. Curve a, b, c and d correspond to the half-cells assembled by sample a, b, c and d.

According to the previous report, the Li-ion diffusion coefficient can be calculated by the following equation [35]

$$D_{Li} = \frac{(RT)^2}{2(An^2F^2C_{Li}\sigma)^2} \quad (1)$$

Where A is the surface area of the electrode (0.785 cm^2), n the number of electrons transferred in the half-reaction for the redox couple, R the gas constant (8.314 J mol^{-1} K^{-1}), T the absolute temperature (298 K), F the Faraday constant (96500 C mol^{-1}), C_{Li} the concentration of lithium ion in solid (4.37 × 10^{-3} mol cm^{-3}), σ is the Warburg factor which can be estimated using the following equation[36].

$$Z_{re} = R_s + R_{ct} + \sigma \omega^{-1/2} \quad (2)$$

Where Z_{re} is the real part of the impedance (here is Z') ; R_s the resistance of electrolyte; R_{ct} the charge transfer resistance and ω is the angular frequency in the low frequency region. The typical curve of Z_{re} against the reciprocal root square of the lower angular frequencies ($\omega^{-1/2}$) for these four samples is shown in Fig. 9c, thus, the value of σ could be obtained directly. The lithium diffusion coefficients for electrode a, b, c and d were calculated to be 3.69×10^{-14}, 5.53×10^{-14}, 1.46×10^{-14} and 1.48×10^{-14} cm^2 s^{-1}, respectively. The calculated values of lithium diffusion coefficient were very close to the previously reported data of 3.0×10^{-14} cm^2 s^{-1} for the LTO prepared by a solid-state method [37]. Thus, electrode b exhibited the largest lithium diffusion coefficient among all samples, which indicated that sample b had the highest electrochemical activity among all synthesized samples. Also, this result strongly demonstrated that a proper amount of doped Pb in LTO could accelerate the lithium ion mobility, which was favorable for improving the electrochemical performance of LTO.

Although the fact that a proper amount of doped metal may increase the electrochemical performance of LTO has been reported in many published papers, the real role of the doped metal in augmenting the electrochemical behavior of LTO still remained unclear. In a summary, so far three reasons have been proposed to explain the role of doped metal in affecting the electrochemical performance of LTO. (1) Varying the lattice parameters of LTO. For example, Ouyang's research group [38] thought that some Ti^{4+} in LTO were substituted by Ce^{3+} ions, which might lead to the expansion of the lattice parameter for the Ce^{3+}-doped LTO. And the expanded volume of unit cell could facilitate fast Li^+ intercalation/extraction during charge-discharge processes, showing improved high-rate performance. (2) Enhancing the electronic conductivity of LTO. For instance, Zhang and his co-workers [39] thought that the significantly enhanced electrochemical behavior of Sc doped LTO was mainly attributed to the highly improved electrical conductivity. (3) Taking part in the Li ion intercalation/de-intercalation process. For example, Wang's group [40] considered that the high capacity of Fe_2O_3 modified LTO should be ascribed to the reduction of Fe_2O_3 to $Li_xFe_2O_3$ during the intercalation process since Fe_2O_3 itself could also be used as anode material of LIBs. As for this Pb-doped LTO anode, the well-defined crystal structure (Fig.1), the relatively uniform particle size distribution (Fig.6), the rearrangement of electronic charge around the constituent atoms of LTO (Fig. 5a and 5b), the lowered charge transfer resistance (Fig. 5a) as well as the larger lithium diffusion coefficient (Fig. 9c) should be mainly responsible for the enhanced electrochemical performance of sample b as compared to other samples.

4. CONCLUSIONS

For the first time, Pb-doped LTO particles were prepared by a solution-drying-calcination (SDC) method using lead acetate as the dopant. In this preliminary work, the influence of Pb to Ti

atomic ratio on the properties of the synthesized samples was systematically investigated. The XRD and SEM results indicated that the doped Pb could significantly affect both the crystallinity and the morphologies of the resultant samples. XPS results indicated that a proper amount of Pb doped into LTO may generate a rearrangement of electronic charge around the constituent atoms of LTO, which may further influence both the migration rate and migration direction of lithium ions. Electrochemical measurement results demonstrated that sample b exhibited a high specific capacity of 169 mAh g^{-1} after 20 cycles at 0.2 C rate, which was close to the theoretical value of 175 mAh g^{-1} of LTO. Using a cheaper dopant of lead acetate to fabricate of a novel metal doped LTO of Pb-doped LTO was the main contribution of this work, which was believed to be suitable for the large scale production of metal doped LTO due to its lower preparation cost and simple production process.

ACKNOWLEDGMENTS

This work was financially supported by National Natural Science Foundation of China (No. 21676022 & 21173066), the State Key Program of National Natural Science of China (21236003), Natural Science Foundation of Hebei Province of China (No. B2011205014 and B2015205150), the Fundamental Research Funds for the Central Universities (JD1612 and YS1406), BUCT Fund for Disciplines Construction and Development (No. XK1531).

References

1. X. Lu, L. Gu, Y. S. Hu, H. C. Chiu, H. Li, G. P. Demopoulos and L. Chen, *J. Am. Chem. Soc.*, 137 (2015) 1581.
2. M. R. Jo, J. Jung, G. H. Lee, Y. Kim, K. Song, J. Yang, J. S. Chae, K. C. Roh, Y. I. Kim, W. S. Yoon and Y. M. Kang, *Nano. Energy.*, 19 (2016) 246.
3. K. Ding, J. Zhao, J. Zhou, Y. Zhao, Y. Chen, L. Liu, L. Wang, X. He and Z. Guo, *Mater. Chem. Phys.*, 177 (2016) 31.
4. H. Z. Li, L. Y. Yang, J. Liu, S. T. Li, L. B. Fang, Y. K. Lu, H. R. Yang, S. L. Liu and M. Lei, *J. Power. Sources.*, 324 (2016) 780.
5. H. Wang, Z. Xua, H. Yia, H. Wei, Z. Guo and X. Wang, *Nano. Energy.*, 7 (2014) 86.
6. H. K. Han, C. Loka, Y. M. Yang, J. H. Kim, S. W. Moon, J. S. Cho and K. S. Lee, *J. Power. Sources.*, 281 (2015) 293.
7. X. Bai, B. Wang, H. Wang and J. Jiang, *J. Alloy. Compd.*, 628 (2015) 407.
8. X. Y. Feng, X. Li, M. Tang, A. Gan and Y. Y. Hu, *J. Power. Sources.*, 354 (2017) 172.
9. M. Lu, H. Yang, Y. Zhang, G. Wang and S. Zhuang, *J. Power. Sources.*, 349 (2017) 52.
10. T. P. Zhou, X. Y. Feng, X. Guo, W. W. Wu, S. Cheng and H. F. Xiang, *Electrochim. Acta.*, 174 (2015) 369.
11. M. Krajewski, M. Michalska, B. Hamankiewicz, D. Ziolkowska, K. P. Korona, J. B. Jasinski, M. Kaminska, L. Lipinska and A. Czerwinski, *J. Power. Sources.*, 245 (2014) 764.
12. Q. Zhang, Y. Liu, H. Lu, D. Tang, C. Ouyang and L. Zhang, *Electrochim. Acta.*, 189 (2016) 147.
13. Q. Zhang, M. G. Verde, J. K. Seo, X. Li and Y. S. Meng, *J. Power. Sources.*, 280 (2015) 355.
14. Q. Zhang, C. Zhang, B. Li, S. Kang, X. Li and Y. Wang, *Electrochim. Acta.*, 98 (2013) 146.
15. K. Ding, W. Li, Q. Wang, S. Wei and Z. Guo, *J. Nanosci. Nanotechno.*, 12(2012) 3813.
16. K. Ding, H. Gu, C. Zheng, L. Liu, L. Liu, X. Yan and Z. Guo, *Electrochim. Acta.*, 146 (2014) 585.
17. X. B. Wang, W. F. Zhu, X. Wei, Y. X. Zhang and H. H. Chen, Mat. Sci. Eng. B-Solid., 185 (2014) 1.
18. S. Sharmila, B. Senthilkumar, V. D. Nithya, K. Vediappan, C. W. Lee and R. K. Selvan, *J. Phys. Chem. Solids.*, 74 (2013) 1515.

19. K. Ding, J. Zhao, J. Zhou, Y. Zhao, Y. Chen, Y. Zhang, B. Wei, L. Wang and X. He. *Int. J. Electrochem. Sci.*, 11 (2016) 446.
20. T. F. Yia, S. Y. Yang, X. Y. Li, J. H. Yao, Y. R. Zhu and R. S. Zhu, *J. Power. Sources.*, 246 (2014) 505.
21. J. P. Han, B. Zhang, X. Bai, L. Y. Wang, Y. X. Qi, N. Lun and Y. J. Bai, *J. Power. Sources.*, 354 (2017) 16.
22. Y. Shi, L. Wen, F. Li and H. M. Cheng, *J. Power. Sources.*, 196 (2011) 8610.
23. V. Batra, C.V. Ramana and S. Kotru, *Appl. Surf. Sci.*, 379 (2016) 191.
24. B. Zheng, W. Hua, Y. Yue and Z. Gao, *J. Catal.*, 232 (2005) 143.
25. T. F. Yi, H. Liu, Y. R. Zhu, L. J. Jiang, Y. Xie and R. S. Zhu, *J. Power. Sources.*, 215 (2012) 258.
26. K. Ding, Y. Zhao, M. Zhao, Y. Li, J. Zhao, Y. Chen and Q. Wang, *Int. J. Electrochem. Sci.*, 10 (2015) 7917.
27. N. Cao, Z. Song, Q. Liang, X. Gao and X. Qin, *Electrochim. Acta.*, 235 (2017) 200.
28. H. P. Liu, G. W. Wen, S. F. Bi, C. Y. Wang, J. M. Hao and P. Gao, *Electrochim. Acta.*, 192 (2016) 38.
29. K. Ding, J. Zhao, Y. Sun, Y. Chen, B. Wei, Y. Zhang and J. Pan, *Ceram. Int.*, 42 (2016) 19187.
30. L. Gao, W. Jiang, W. Wei, J. Yan and Z. Tang, *Mater. Lett.*, 131 (2014) 324.
31. W. Li, H. Wang, M. Chen, J. Gao, X. Li, W. Ge, M. Qu, A. Wei, L. Zhang and Z. F. Liu, *Electrochim. Acta.*, 188 (2016) 499.
32. K. Ding, Y. zhao, L. Liu, Y. Li, L. Liu, L.Wang, X. He and Z. Guo, *Electrochim. Acta.*, 176 (2015) 240.
33. K. Ding, J. Zhao, M. Zhao, Y. Chen, Y. Zhao and J. Zhou, *Int. J. Electrochem. Sci.*, 11 (2016) 2513.
34. G. Zhang, W. Li, H. Yang, Y. Wang, S. B. Rapole, Y. Cao, C. Zheng, K. Ding and Z. Guo, *J. New.Mat. Electr. Sys.*, 16(2013) 025.
35. T. F. Yi, H. Liu, Y. R. Zhu, L. J. Jiang, Y. Xie and R. S. Zhu, *J. Power. Sources.*, 215 (2012) 258.
36. Q. Cao, H. P. Zhang, G. J. Wang, Q. Xia, Y. P. Wu and H. Q. Wu, *Electrochem. Commun.*, 9 (2007) 1228.
37. W. Liu, D. Shao, G. Luo, Q. Gao, G. Yan, J. He, D. Chen, X. Yu and Y. Fang, *Electrochim. Acta.*, 133 (2014) 578.
38. Q. Zhang, Y. Liu, H. Lu, D. Tang, C. Ouyang and L. Zhang, *Electrochim. Acta.*, 189 (2016) 147.
39. Y. Zhang, C. Zhang, Y. Lin , D. B. Xiong, D. Wang, X. Wu and D. He, *J. Power. Sources.*, 250 (2014) 50.
40. B. Wang, J. Cao, Y. Liu, T. Zeng and L. Li, *J. Alloy. Compd.*, 587 (2014) 21.